Structural Studies of the β-Glycosidase from *Sulfolobus solfataricus* in Complex with Covalently and Noncovalently Bound Inhibitors†

Tracey M. Gloster,‡ Shirley Roberts,‡ Valérie M-A. Ducros,‡ Giuseppe Perugino,⊥ Mosè Rossi,⊥,§ Roland Hoos,∥ Marco Moracci,⊥ Andrea Vasella,∥ and Gideon J. Davies*,‡

Structural Biology Laboratory, Department of Chemistry, The University of York, Heslington, York YO10 5YW, United Kingdom, Institute of Protein Biochemistry−CNR, Via P. Castellino 111, 80131 Naples, Italy, Dipartimento di Chimica Biologica, Università di Napoli "Federico II", Via Mezzocannone 16, 80134 Naples, Italy, and Laboratorium für Organische Chemie, HCI H 317, ETH-Hönggerberg, CH-8093 Zürich, Switzerland

Received February 13, 2004; Revised Manuscript Received March 18, 2004

ABSTRACT: Transition-state mimicry is increasingly important both to understand enzyme mechanism and to direct the synthesis of putative therapeutic agents. X-ray crystallography is able to provide vital information on the interactions between an enzyme and the potential inhibitor. Here we report the structures, at approximately 2 Å resolution, of a family GH1 β-glycosidase from the hyperthermophilic archaeon *Sulfolobus solfataricus*, in complex with both covalently (derived from 2-fluoro-glycosides) and noncovalently (hydroximolactam) bound inhibitors. The enzyme has broad specificity, accommodating both *gluco*- and *galacto*-configured substrates, and the crystallographic data demonstrate that the only difference in the way these ligands bind lies in the interactions between Gln18, Glu432, and Trp433, and the hydroxyl group at the O3 and O4 positions. Inhibition by the differently configured ligands was also shown to be extremely similar, with K_i values of 1.04 and 1.08 μM for the *gluco* and *galacto* epimers, respectively. The noncovalently bound inhibitors have a trigonal anomeric carbon, adopt a $^4H_3$ (half-chair) conformation, and an interaction is formed between O2 and the catalytic nucleophile, all of which contribute to (partial) mimicry of the oxocarbenium-ion-like transition state. The inhibition of the β-glycosidase from *S. solfataricus* by hydroximolactams is discussed in light of the emerging work on family GH1 glycosidase inhibition by a spectrum of putative transition-state mimics.

Glycoside hydrolases have been shown, through the comparison of uncatalyzed (k_{uncat}) and catalyzed (k_{cat}) reaction rates under similar conditions, to accelerate the rate of glycosidic bond hydrolysis by a factor of approximately 10^{17}, making them among the most proficient of enzymes (*1*). One may thus estimate (as described in ref *2*), taking into account K_M values around 10^{-5} M, that the resultant dissociation constant of the enzyme−substrate (ES) complex at the transition state is around 10^{-22} M (*1*). The high affinity for the transition state makes glycosidases particularly rewarding targets for inhibitor design through mimicry of this transition state. Indeed, a number of successful therapeutic agents, including Acarbose, Miglitol, *N*-butyl-deoxynojirimycin, Tamiflu and Relenza, have been targeted at this enzyme class (for example, see ref *3*).

Enzymes that catalyze the hydrolysis of glycosides have been classified into over 90 families on the basis of amino acid sequence similarities.[1] Within these families, "classical" hydrolysis of the glycosidic bond occurs via two mechanisms, which results in either net retention or inversion of configuration at the anomeric carbon. An *exo*-β-glycosidase, Ssβ-Glc1,[2] from *Sulfolobus solfataricus* (an extremely thermoacidophilic archaeon that optimally grows in hot springs at around 80 °C and pH 3), derived from the *lacS* gene, has been classified into glycoside hydrolase family GH1 (*4*). The three-dimensional structure of the native enzyme was first reported at 2.6 Å resolution (*5*). A large number of GH1 structures have now been reported; all are nonreducing-end specific *exo*-glycosidases with a wide variety of both glycon and aglycon specificities (for example, see refs *6*−*12*). Most recently, the *Thermotoga maritima* GH1 enzyme was solved in complex with two imino-sugar inhibitors that, in harness with calorimetric measurements, provide provocative insight into enzyme inhibition (*13*).

Family GH1 members perform catalysis with retention via a double-displacement mechanism through a covalent glycosyl−enzyme intermediate. During the first step of the canonical retention mechanism, the acid/base (invariably Asp or Glu) protonates the glycosidic oxygen to assist departure of the (poor) leaving group, with migration of the electro-

† The work in Naples was supported by an Agenzia Spaziale Italiana project, contract no. I/R/365/02, and by a MIUR project, contract no. RBAU015B47, "Folding di proteine: l'altra metà del codice genetico". The work in York was supported by the EPSRC and the BBSRC. G.J.D. is a Royal Society University Research fellow.

* To whom correspondence should be addressed. Tel.: +44 1904 328260. Fax: +44 1904 328266. E-mail: davies@ysbl.york.ac.uk.

‡ The University of York.

⊥ Institute of Protein Biochemistry−CNR.

§ Università di Napoli "Federico II".

∥ ETH-Hönggerberg.

[1] http://afmb.cnrs-mrs.fr/~cazy/CAZY/index.html.

[2] Abbreviations: Ssβ-Glc1, β-glycosidase from *Sulfolobus solfataricus*; 2F-Glc, 2-deoxy-2-fluoro-glucose; 2F-Gal, 2-deoxy-2-fluoro-galactose; rms, root-mean-square; RMSD, root-mean-square deviation; GH1, glycoside hydrolase from family 1.

10.1021/bi049666m CCC: $27.50
Published on Web 04/29/2004

Scheme 1: Putative Oxocarbenium-Ion-Like Transition State Formed during Both the Glycosylation and Deglycosylation Steps of Glycoside Hydrolysis with Net Retention of Anomeric Configuration[a]

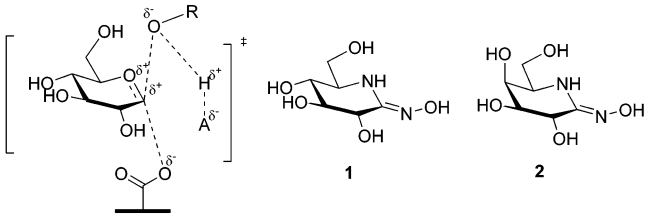

[a] A−H represents the catalytic acid/base and/or the leaving group. Crystallographic studies were conducted using putative transition-state analogues D-glucohydroximolactam **1** and D-galactohydroximolactam **2**.

philic anomeric center to the nucleophile, resulting in formation of the covalent intermediate. In the second chemical step, the acid/base now acts as a Brønsted base, deprotonating the hydrolytic water which then attacks this glycosyl−enzyme intermediate, resulting in release of product with net retention of anomeric configuration. Both steps go via transition states with substantial oxocarbenium ion character (Scheme 1). At, or near to, this transition state, the anomeric center must display partial sp^2 hybridization and charge delocalization which is manifested primarily at the endocyclic oxygen (O5) and the anomeric carbon (C1).

To study the structural aspects of enzyme inhibition and to elucidate some of the specific features of the Ssβ-Glc1 enzyme, we have studied the three-dimensional structures of the enzyme in complex with the transition-state analogues (containing an sp^2 anomeric center and corresponding $^4H_3$ conformation) D-glucohydroximolactam (**1**) and D-galactohydroximolactam (**2**) as well as with the corresponding trapped covalent−enzyme intermediates, 2-deoxy-2-fluoro-glucose (2F-Glc) and 2-deoxy-2-fluoro-galactose (2F-Gal). As with many GH1 enzymes, Ssβ-Glc1 is known to have broad specificity for a number of saccharides (*7*), and the data provide insights into the interactions of both the *gluco*- and *galacto*-derived ligands which could help direct and inform strategies for enzyme exploitation.

MATERIALS AND METHODS

Protein Expression, Purification, and Crystallization. Ssβ-Glc1 was expressed and purified essentially as described previously (*7*). The enzyme (at 10−13 mg mL^{-1} in 25 mM HEPES, pH 7.0) was crystallized by vapor diffusion in sitting drops from 11−14% (w/v) PEG 4000, 0.1 M sodium acetate, pH 4.6, and 0.2 M ammonium acetate. To obtain complexes of the enzyme with *galacto*-configured ligands, 10−20 mM 2,4-dinitrophenyl 2-deoxy-2-fluoro-galactoside (generous donation from Professor S. G. Withers, University of British Columbia) or 10 mM **2** (synthesis described in refs *14*, *15*) were added to Ssβ-Glc1 and incubated for 2 h prior to crystallization in the same conditions as native Ssβ-Glc1. Smaller quantities of the corresponding *gluco*-configured ligands necessitated an alternative strategy, and minute solid amounts of 2,4-dinitrophenyl 2-deoxy-2-fluoro-glucoside (again a generous donation from Professor S. G. Withers, University of British Columbia) or **1** (synthesis described in refs *16*, *17*) were added to the mother liquor containing native crystals of Ssβ-Glc1 and allowed to soak for 20 min with the crystal under constant observation. All crystals were harvested into a "cryo-protectant" mother liquor (11−14% (w/v) PEG 4000, 0.1 M sodium acetate, pH 4.6, and 0.2 M ammonium acetate, pH 4.6, with the addition of 25% v/v ethylene glycol) and mounted in rayon fiber loops prior to "flash"-freezing in liquid nitrogen.

Data Collection and Processing. Native data were collected to 2.0 Å resolution from a single crystal at 100 K at the ESRF Grenoble, beamline ID14-1. Data were processed and reduced with DENZO and SCALEPACK (*18*). All other calculations used the CCP4 suite of programs (*19*). Crystals belong to space group $P3_121$, with unit cell dimensions $a = b = 168.0$ Å, $c = 94.6$ Å, and $\alpha = \beta = 90°$, $\gamma = 120°$. The structure was solved using AMoRe (*20*), with PDB entry 1gow as the search model. Data were used in the resolution range from 10 to 4 Å, with an outer radius of Patterson integration of 25 Å. Molecular replacement gave two solutions, corresponding to two molecules in the asymmetric unit. This gave $V_M = 3.4$ Å^3 Da^{-1} and a solvent content of approximately 65%. All data for Ssβ-Glc1 in complex with ligands were also collected at the ESRF Grenoble; data for the 2F-Gal complex were collected on beamline ID-29 (to 2.15 Å resolution), and the complexes with 2F-Glc, **1**, and **2** were collected, all to 1.95 Å resolution, on beamline ID14-4. Small rigid-body motions meant that AmoRe (*20*) (resolution range from 10 to 4 Å, radius of integration 25 Å) was required to solve the structures with **1** and 2F-Glc, using the native refined structure as the search model.

Model Refinement. Five percent of the observations (the same observations for each data set) were set aside for cross validation (*21*) and were used to monitor refinement strategies such as geometric and temperature factor restraint values. Manual corrections of the model using X-FIT in QUANTA (Accelrys, San Diego, CA) were interspersed with cycles of least-squares refinement using the maximum likelihood program REFMAC (*22*). Water molecules were added automatically using ARP/wARP (*23*) and manually using X-SOLVATE in QUANTA. All were inspected prior to deposition. Energy-minimized ligand molecules were created using the CHARMm function in QUANTA, and dictionaries were created using the "monomer library sketcher" in the CCP4 suite. The models were validated using PROCHECK (*24*), and the coordinates were deposited with the Macromolecular Structure Database at the European Bioinformatics Institute (http://autodep.ebi.ac.uk); PDB codes are given in Table 1.

Enzyme Inhibition. Kinetic studies were conducted by monitoring the change in UV/visible absorbance with a Cintra 10 spectrophotometer, equipped with a Thermocell Peltier power supply. All experiments were performed at 37 °C, with a 10 min equilibration period for each sample prior to addition of Ssβ-Glc1. Ssβ-Glc1 activity was measured using between 0.05 and 4 mM 4-nitrophenyl β-D-glucopyranoside as substrate; all reactions were carried out in 50 mM sodium phosphate buffer, pH 6.5, in a total volume of 1 mL. The reaction was initiated by addition of 10 μL of Ssβ-Glc1 to give a final concentration of 13 nM. 4-Nitrophenol release was monitored continuously at 405 nM ($\epsilon_{405} = 6570$ M^{-1} cm^{-1}, calculated using the assay conditions according to the method described in ref *25*) for a 600 s period. Rates were taken as the slope of the line between

Table 1: Data Quality and Structure Refinement Statistics

	native	2F-Gal	2F-Glc	**1**	**2**
resolution (Å)	40.0−2.02	30.0−2.15	30−1.95	40.0−1.95	40.0−1.95
(outer shell)	(2.09−2.02)	(2.23−2.15)	(2.02−1.95)	(2.02−1.95)	(2.02−1.95)
ESRF beamline	ID14-1	ID29	ID14-4	ID14-4	ID14-4
R_{merge}	0.069 (0.461)	0.117 (0.455)	0.074 (0.339)	0.102 (0.371)	0.064 (0.415)
completeness (%)	99.0 (98.7)	99.9 (100.0)	99.9 (100.0)	99.0 (99.2)	100.0 (100.0)
multiplicity	4.89 (4.44)	5.89 (5.86)	6.2 (6.2)	5.3 (4.4)	7.13 (7.06)
mean I/σ	17.3 (3.15)	10.1 (2.82)	17.5 (6.03)	9.15 (2.95)	17.2 (4.48)
no. of unique reflections	99 428	85 809	112 688	110 958	113 580
R_{cryst}	0.19	0.19	0.19	0.19	0.20
R_{free}	0.23	0.23	0.23	0.23	0.24
RMSD bond (Å)	0.013	0.015	0.014	0.014	0.015
RMSD angle (°)	1.3	1.4	1.4	1.4	1.5
RMSD chiral (Å$^{3)}$	0.097	0.099	0.107	0.109	0.117
no. of protein atoms	7950	7916	7962	7954	7994
no. of ligand atoms	na	22	22	26	26
no. of water atoms	866	625	758	881	914
average protein main-chain *B* factor (Å^2)	36	41	32	34	36
average protein side-chain *B* factor (Å^2)	37	42	33	34	36
average ligand *B* factor (Å^2)	na	40	23	28	29
average water *B* factor (Å^2)	46	47	43	44	48
PDB code	1uwq	1uwr	1uws	1uwu	1uwt

200 and 300 s. The data were fit to the Michaelis−Menten equation using GraFit (*26*).

To determine inhibitor K_i values, reactions were carried out as described above with the addition of between 0.3 and 4 μM **1** or **2** to a range of substrate concentrations ranging from 0.08 to 4.5 mM. Data for each inhibitor concentration were fitted to the Michaelis−Menten equation using GraFit (*26*) to obtain K_M and V_{max} values. The apparent K_M at different inhibitor concentrations was plotted against the inhibitor concentration. The $-K_i$ was taken as the value where the best-fit line through the points crossed the *x* axis.

The presence of 2 μM (or greater) **1** in a reaction mixture containing 65 nM Ssβ-Glc1 and 0.2 mM (or lower) substrate gave a partially curved profile when absorbance was plotted against time, making it difficult to measure a single rate accurately. This is partially indicative of "slow-onset inhibition". A 5-fold dilution of Ssβ-Glc1 reduced the rates, and a single steady-state slope was easier to determine. All reactions were therefore carried out at a lower enzyme concentration, and the rate was taken between an arbitrary time period of 200−300 s, during which time any initially fast rates had equilibrated. Rates between 200 and 300 s were linear for all reactions, and the correlation coefficient for the slopes were monitored.

RESULTS

Data were collected for native Ssβ-Glc1 to 2.0 Å resolution. The data are 99% complete, with an overall R_{merge} of 0.069, a mean I/σ_I of 17.3, and a mean multiplicity of 4.9 observations/reflection. The model was refined to a final R_{cryst} of 0.192 and R_{free} of 0.226 (Table 1). The asymmetric unit contains two protein molecules, each of 489 residues. A total of 866 solvent molecules have been included in the model. Two loop regions in chain B (96−97 and 301−302) and one loop region in chain A (301−302) could not be built due to disordered density. The native structure is similar to that described previously (*5*), although a number of sequence conflicts in the original PDB deposition have been rectified (Val82, Ile87, Leu146, and Ile190 had previously erroneously been included as Ser, Gln, Gln, and Thr, respectively). The native structure reported here and that described previously overlap with a main-chain rms of 0.37 Å, calculated using LSQKAB from the CCP4 suite. The mass of Ssβ-Glc1 measured using quadrupole time-of-flight electrospray mass spectrometry (Applied Biosystems QSTAR) (56689.6 Da) was in good agreement with the calculated mass for the correct sequence (56691.6 Da). Ssβ-Glc1 adopts the classic $(\beta/\alpha)_8$ barrel fold, as expected for a clan GH-A glycoside hydrolase. The acid/base (Glu206) and nucleophile (Glu387) are found on β-strands four and seven, respectively (*27*) (Figure 1).

Inhibition by gluco- and galacto-Hydroximolactams. Hydroximolactams display characteristics of the transition state, as they contain a trigonal anomeric carbon and thus adopt a $^4H_3$ conformation. Furthermore, hydroximolactams also contain a hydroxyl substituent at C2 (which many other inhibitors do not possess), which should be important for transition-state mimicry, given that interactions at the 2-position of many β-glycosidases are estimated to contribute >40 kJ mol^{-1} to transition-state binding (*28*, *29*).

Inhibition constants were determined using 4-nitrophenyl β-D-glucopyranoside as substrate (Figure 2). Kinetic constants for Ssβ-Glc1, determined at pH 6.5 (the pH optimum for Ssβ-Glc1 catalysis (*27*)) and at 37 °C, gave a K_M of 0.16 mM and a k_{cat} of 4.2 s^{-1}. Precedence from other related enzymes suggests that the low apparent K_M may be a "kinetic" effect from the presence of a reasonably good leaving group, and thus k_3 (deglycosylation) may be (partially) rate-limiting (see, for example, ref *30*). Although the k_{cat} is some 128 times lower than that recorded at 65 °C (*25*), this is consistent with Wolfenden's estimates of $Q_{10} = 6$ for glycoside hydrolysis (*1*).

Both **1** and **2** are shown to be competitive inhibitors of Ssβ-Glc1, with similar K_i values of 1.04 ± 0.16 and 1.08 ± 0.17 μM, respectively. They also show some features of "slow-onset inhibition" (see Materials and Methods). The molecular basis for slow-onset inhibition will most likely be case-specific, and there is much, often confusing, speculation in the literature. On the basis of our work on the pH dependence of a related GH1 enzyme, we hypothesized that

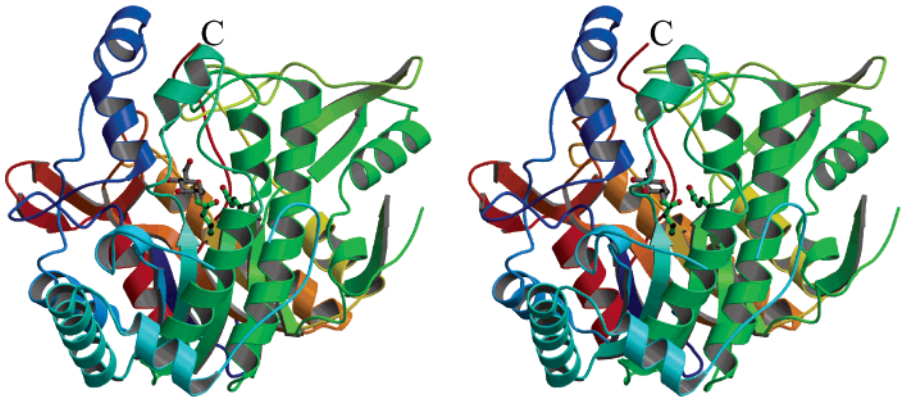

FIGURE 1: Divergent ("wall-eyed") stereo ribbon representation of a Ssβ-Glc1 monomer (the protein is tetrameric in solution) drawn using MOLSCRIPT (*51*). The nucleophile (Glu387), acid/base (Glu206), and 2-deoxy-2-fluoro-glucosyl−enzyme intermediate covalently bound to the nucleophile are shown in "ball-and-stick" representation.

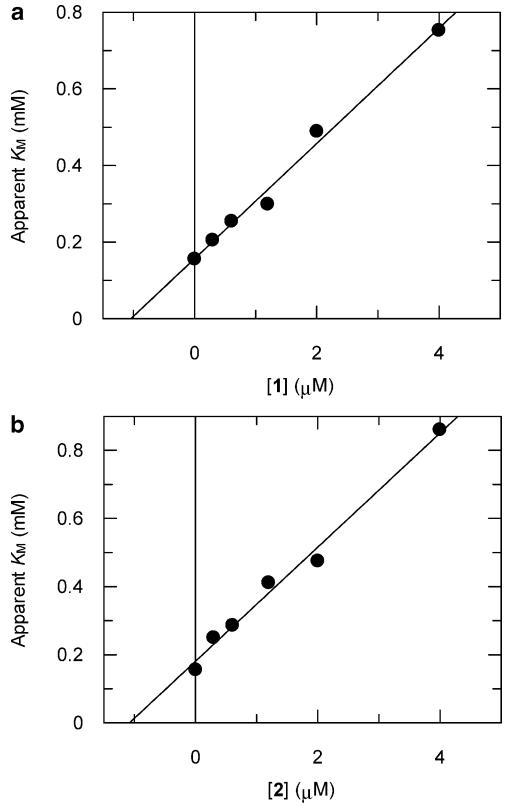

FIGURE 2: Plot of apparent K_M against inhibitor concentration for (a) **1** and (b) **2**. Experiments were conducted using between 0.05 and 4 mM 4-nitrophenyl β-D-glucopyranoside as substrate and concentrations of **1** or **2** between 0.3 and 4 μM.

changes in protonation state (of enzyme or inhibitor) and any subsequent structural rearrangements may play a role in the slow-onset inhibition of glycosidases, especially for those systems that require "non-native" protonation states for optimal inhibition (*13*). Clearly, much work is required to dissect these unusual "artifacts" of inhibition.

X-ray diffraction data were collected for Ssβ-Glc1 in complex with **1** and **2** to 1.95 Å resolution. Data for the complex with **1** are 99% complete, with an overall R_{merge} of 0.102, a mean I/σ_I of 9.15, and a multiplicity of 5.3 observations/reflection. The model was refined to a final R_{cryst} of 0.191 and R_{free} of 0.230. The data for the complex with **2** are 100% complete, with an overall R_{merge} of 0.064, a mean I/σ_I of 17.2, and a multiplicity of 7.13 observations/reflection. The model was refined to a final R_{cryst} of 0.199 and R_{free} of 0.238. Partial disorder is observed in the loop regions of 96−97 and 300−303 in both molecules of each complex.

Both **1** and **2** bind in the −1 subsite, of both molecules in the asymmetric unit, in their respective complexes (Figures 3 and 4). Both display a potential transition state mimicking $^4H_3$ conformation; the double bond between C1 and the nitrogen atom of the hydroximolactam restrains C5, N1, C1, C2, and N2 to lie a plane. A superposition of the two complexes shows that the active-site residues are in identical positions. Trp433, Trp151, and Trp425 all make hydrophobic interactions with the ligands. The C6−OH group hydrogen-bonds to Glu432 (Oϵ2) in both cases. The C2−OH group interacts with both oxygen atoms of the nucleophile and the nitrogen of Asn205. The hydroximo nitrogen atom hydrogen-bonds with both oxygen atoms of the acid/base (Glu206). The oxygen of the hydroximo group must hydrogen-bond to solvent water, but at similar (one sigma) electron density level we observe solvent disorder to differing degrees. In the complex with **1**, two water molecules are observed in one molecule of the asymmetric unit, but only one is seen in the B molecule. For the complex with **2**, we observe a single water molecule coordinating to the oxygen in the B molecule, but in the A molecule this can be seen only at a low contour level. O3 of the sugar ring interacts with the oxygen of Gln18 and Nϵ2 of His150. The acid/base Glu206 is close to the mean plane of the ring of the inhibitors, as shown in Figures 3 and 4, consistent with their "anti"-protonating trajectory (with respect to the plane defined by O1, C1, and H1 of the pyranose ring of the substrate) (*31*, *32*).

The only differences in the interactions made in the active site reflect the *gluco* and *galacto* configurations of the hydroxyl group at C4. Compound **2** interacts with Oϵ2 of Glu432 and the nitrogen of Trp433, whereas the O4 of **1** hydrogen-bonds with Oϵ1 of Glu432 and the nitrogen of Gln18. The nitrogen of Trp433 hydrogen-bonds to the O3 atom of **1** rather than with O4 as observed for the complex with **2**. Superposition of the native structure with the noncovalently bound complexes shows that there is movement of the acid/base, Glu206, to accommodate the hydroximo group. All other residues appear to be in the same position as the native structure.

Structures in Complex with Trapped 2-Fluoro Glycosyl−Enzyme Intermediates. One of the most significant achievements in retaining glycosidase research is the trapping of

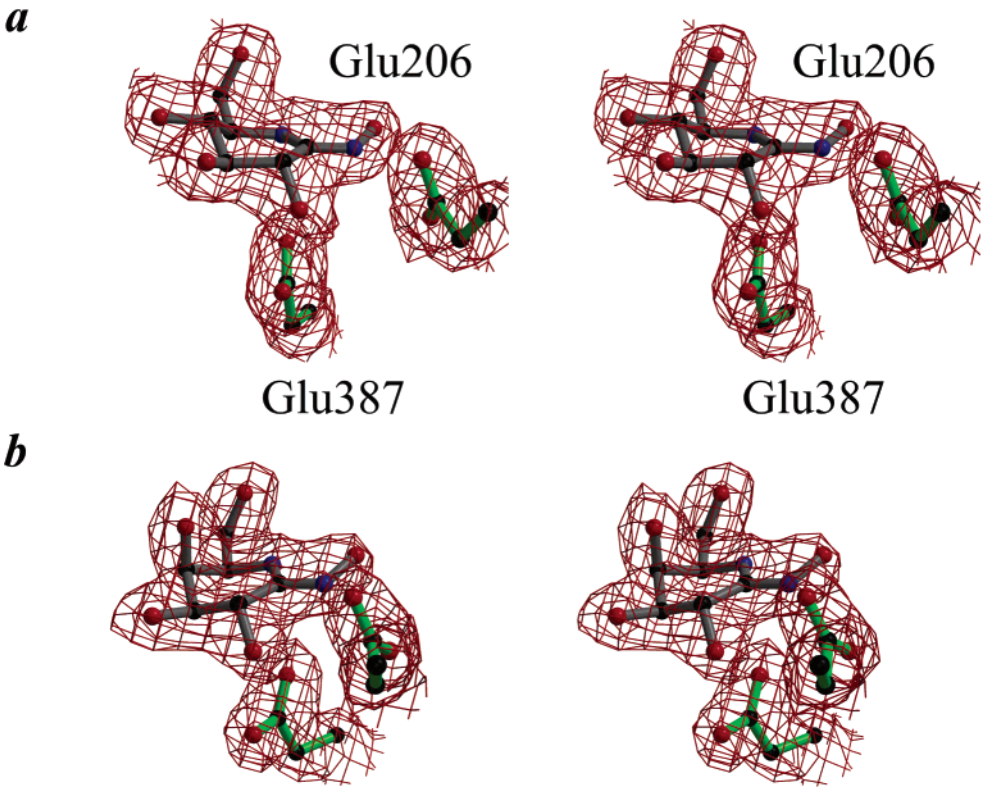

FIGURE 3: Divergent ("wall-eyed") stereo "ball-and-stick" representation of noncovalently bound inhibitors (a) **1** and (b) **2**. Observed electron density for the maximum likelihood weighted $2F_{obs} - F_{calc}$ map is contoured at 1σ (~0.25 e Å^{-3}); figures were drawn using BOBSCRIPT (*52*).

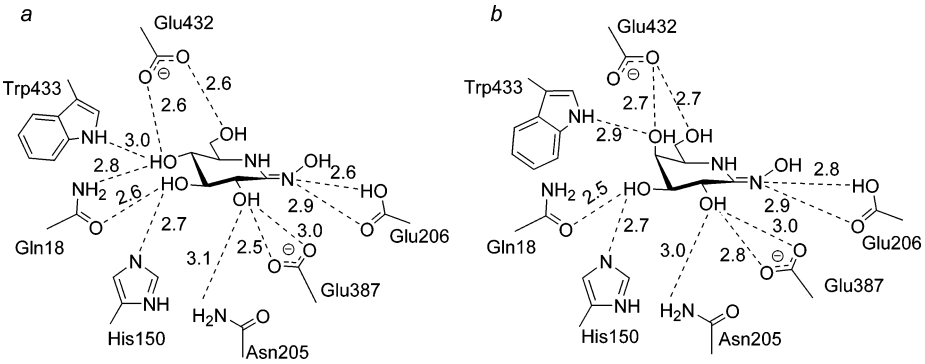

FIGURE 4: Schematic diagram of the interactions between (a) **1** and (b) **2** and Ssβ-Glc1.

long-lived, but catalytically competent, covalent intermediates through the use of 2-deoxy-2-fluoro glycosides (for example, see ref *33*). These reagents facilitate accumulation of a stable intermediate through both inductive destabilization of the oxocarbenium-ion-like transition state and loss of critical O2 interactions. When used in conjunction with a good leaving group (such as dinitrophenol or fluoride), 2-fluoro substrates allow accumulation of the intermediate and its subsequent observation by both mass spectrometry and X-ray crystallography (recent examples from the authors' laboratory include a family 1 β-glucosidase from *T. maritima* (*13*) and a family 26 β-mannanase from *Cellvibrio japonicus* (the organism originally known as *Pseudomonas fluorescens* subsp. cellulosa and then *Pseudomonas cellulosa*) (*34*)).

Data were collected for Ssβ-Glc1 in complex with 2F-Gal and 2F-Glc to resolutions of 2.15 and 1.95 Å, respectively. The data for the 2F-Gal complex are 99.9% complete, with an overall R_{merge} of 0.117, a mean I/σ_I of 10.1, and a multiplicity of 5.9 observations/reflection. The model was refined to a final R_{cryst} of 0.188 and R_{free} of 0.229. The data for Ssβ-Glc1 in complex with 2F-Glc are 99.9% complete, with an overall R_{merge} of 0.074, a mean I/σ_I of 17.5, and a multiplicity of 6.2 observations/reflection. The model was refined to a final R_{cryst} of 0.191 and R_{free} of 0.231. Both models contain two loop regions (96−97 and 300−303) that could not be built to varying extents in both molecules of the asymmetric unit.

Electron density clearly reveals 2F-Gal and 2F-Glc in their respective structures (Figure 5), each positioned in the −1 subsite of Ssβ-Glc1, covalently bound to the nucleophile, Glu387. Both are in the relaxed $^4C_1$ conformation, typical of the covalent glycosyl-enzyme intermediates observed for β-glucosidases and β-galactosides. A superposition of the two complexes shows that the active-site residues are in identical positions. Both C6−OH groups interact with Glu432 (Oε2) and a water molecule. The endocyclic ring

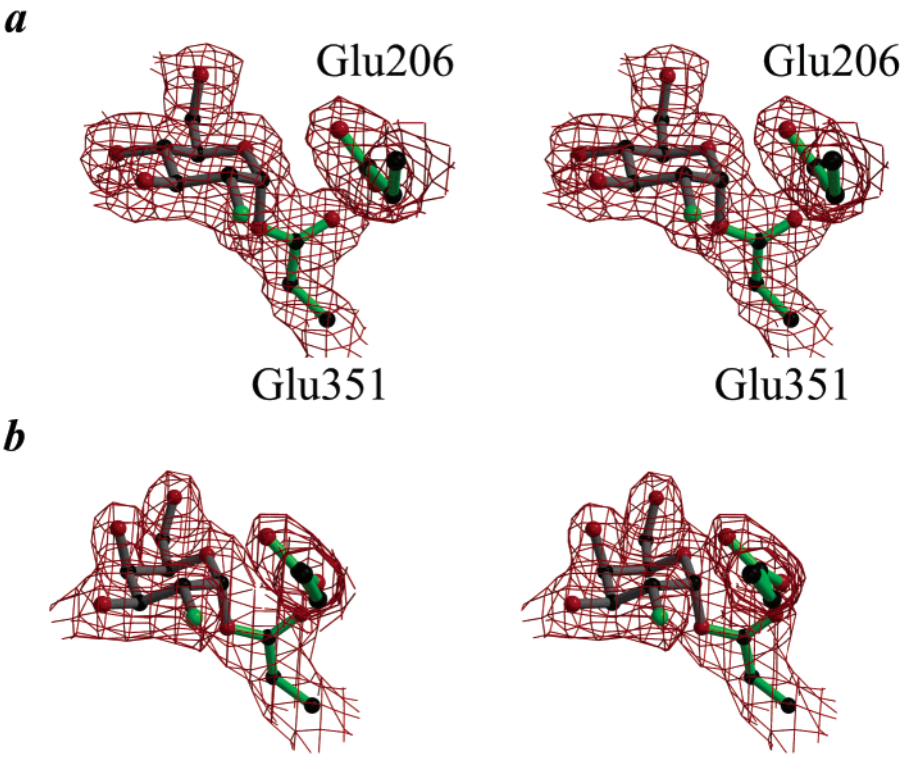

FIGURE 5: Divergent ("wall-eyed") stereo "ball-and-stick" representation of (a) 2-deoxy-2-fluoro-glucose and (b) 2-deoxy-2-fluoro-galactose covalently bound to the nucleophile, Glu387. Observed electron density for the maximum likelihood weighted $2F_{obs} - F_{calc}$ map is contoured at 1σ (~0.25 e Å^{-3}); figures were drawn using BOBSCRIPT (*52*).

oxygen lies close to the oxygen of Tyr322. F2 interacts with both the side-chain amide of Asn205 and the nucleophile. The hydrogen bonds made by O3 with the oxygen of Gln18 and the nitrogen of His150 are also conserved with each inhibitor.

Exactly as observed for inhibition by **1** and **2**, the only difference in the interactions made by the two inhibitors is at the C4 position, where the hydroxyl group takes equatorial and axial configurations in the *gluco* and *galacto* forms, respectively. In both cases O4 interacts with the nitrogen of Trp433. The difference between the accommodation of these 4-epimers is subtle: whereas 2F-Gal hydrogen bonds to the Oϵ2 of Glu432, 2F-Glc interacts with the Oϵ1.

The interactions of the covalent complexes are extremely similar to those observed for **1** and **2** (as shown in Figure 4). Superposition of the covalently bound ligand complexes with the native structure shows that the nucleophile Glu387 of Ssβ-Glc1 has, however, moved to accommodate the covalent linkage to the sugar. The Cα−Cβ bond appears to be in a similar position in both the native structure and the complexes; rotation occurs around the Cβ−Cχ bond to place the Oϵ2 of the nucleophile in covalent intimacy with C1 of the inhibitor and also to avoid destabilizing interactions between F2 of the glycoside and Oϵ1 of Glu387. This latter movement, as observed on many trapped 2-fluoro enzyme intermediates, makes it impossible to draw useful conclusions about the differences in interactions of the hydroxyl group at the 2 position with intermediate and putative transition-state mimics. Tyr322 also rotates upon ligand binding such that it makes a 3.0−3.1 Å interaction with O5 in the trapped intermediate structures. The interaction of an electronegative atom with the O5 of the substrate (in this case intermediate) is a feature of both α- and β-glycosidases (for example, see refs *35*, *36*), although it is more frequently commented upon for α-glucosidases (for example, see ref *37*) and may well contribute significantly to catalysis.

DISCUSSION

Kinetic experiments have shown that Ssβ-Glc1, as with many family GH1 glycosidases (for example, see refs *28*, *30*), is capable of hydrolyzing a number of aryl glycosides, including galactose, fucose, glucose, and xylose, as well as di- and oligosaccharide β-linked glucose derivatives (*7*). This substrate plasticity is particularly important given the application of Ssβ-Glc1 in chemoenzymatic synthesis via transglycosylation and "glycosynthesis", especially since the enzyme is resistant to organic solvent and acidic conditions and shows increased solubility and yield at higher temperatures (*38*). Indeed, the use of a nucleophile mutant, with formate as an external nucleophile, results in the effective synthesis of both 3-*O*-β-linked disaccharides (*25*) and branched oligosaccharides (*39*).

The data presented here show Ssβ-Glc1 in complex with two putative transition-state analogues and with two covalent intermediates, one of each in *gluco* and *galacto* configuration. Kinetics and three-dimensional structure show that Ssβ-Glc1 recognizes *gluco*- and *galacto*-configured substrates almost equally well: the interactions made by the compounds with the enzyme are extremely similar in each case, and the measured K_i values show that they have very similar inhibitory power. The only differences between the accommodation of *gluco* and *galacto* derivatives is that the *gluco* epimer hydrogen-bonds with the Oϵ1 of Glu432, in contrast to the *galacto* epimer, which interacts with Oϵ2. In the case of the noncovalently bound hydroximolactams, an additional difference manifests itself with the Nϵ1 of Trp433, which hydrogen-bonds to the O4 of **2** but with the O3 of **1**. Such

plasticity around the 4 position is not unusual for glycosidases. Not only has it been exploited, for example, with the *Agrobacterium* sp. β-glucosidase Abg glycosynthase mutants (*40*, *41*), but it has also been well characterized structurally, notably on family 20 hexosaminidases (*42*, *43*). GH20 enzymes are able to hydrolyze both terminal *N*-acetyl glucosamine- and *N*-acetyl galactosamine-containing compounds. As with the Gln18 interaction with both O3 and O4 of *gluco*-configured substrates (compound **1** and 2FGlc, described above), Arg162 of the *Streptomyces plicatus* hexosaminidase makes a bifurcated hydrogen bond with both O3 and O4 of *N*-acetyl glucosamine-derived ligands. Upon binding of *N*-acetyl galactosamine, GH20 enzymes lose the arginine interaction to O4 (while maintaining that with O3), exactly as observed here with Gln18 (*42*). Furthermore, as here, it is a glutamate residue (Glu444 in the *S. plicatus* GH20; Glu432 in Ssβ-Glc1) that modifies its interaction to accommodate the axial O4 of the *galacto*-configured substrates (Figure 4b). It would seem, therefore, that the use of single side chains permitting twin interactions with O3 and O4 generates considerable flexibility around these positions to tolerate differently configured ligands, which has been exploited both by nature and for chemoenzymatic synthesis strategies.

In the case of Ssβ-Glc1, plasticity of the interactions around the O3 and O4 positions both explains previous mutagenesis data, in which when Trp433 was mutated there was a much greater effect on the recognition of 2-position *gluco*-configured substrates than on the hydrolysis of mannosides (*44*), and also contributes to the evolving view that recognition of different transition-state conformations for different epimers may be transmitted to distant hydroxyls (*34*). Kinetics of the W433C mutant of Ssβ-Glc1 was analyzed against both *manno*- and *galacto*-derived substrates. Although catalysis was reduced in both cases, considerably less effect was observed for mannoside recognition, with a consequent 25-fold improvement in the ratio of k_{cat}/K_M(Man): k_{cat}/K_M(Gal) compared to the wild-type (*44*). Although interpretation is confused by the change of epimer at two centers (O2 and O4), the work may be consistent with previous proposals that mannoside hydrolysis goes through a $B_{2,5}$ conformation in which the largest conformational difference, to the $^4H_3$ transition state for glucoside hydrolysis, occurs at O3 (*34*). Hence, changes in the interactions around O3 and O4 may, indirectly, change the enzyme's epimeric preference at the 2-position. Modification of the interactions of the "wrong" hydroxyls may represent a powerful way to modulate enzyme specificity. Mutation of Gln18 of Ssβ-Glc1 would shed further light on this area.

1 has previously been shown to be an inhibitor of both α- and β-glucosidases, with K_i values of 16, 0.6, and 3.3 μM for β-glucosidases from almonds, *Agrobacterium faecalis*, and *Caldocellum saccharolyticum*, respectively (*45*), similar to the ~1 μM value observed here. Both **1** and **2** display characteristics typical of the transition state, as they contain a trigonal anomeric carbon and adopt a corresponding $^4H_3$ conformation. K_i values around 1 μM do not appear to reflect great mimicry of the transition state. They are indeed only 100-fold tighter than apparent K_M values of around 0.1 mM for 4-nitrophenyl β-D-glucopyranoside hydrolysis, although such a K_M most likely reflects the deglycosylation step which is rate-limiting, and thus the true K_d for the substrate is likely to be some 100−1000 times higher (*28*, *30*). We have certainly not observed product inhibition on this system, suggesting that K_i values for glucose or galactose must be extremely high. Despite this qualifier, hydroximolactams do not bind tightly. This may reflect their need for "in-plane" *anti* protonation of the exocyclic nitrogen by the acid/base. Given that, at the transition state, the glycosidic oxygen is axial (Scheme 1), the requirement for in-plane protonation of an inhibitor, while generating specificity for *anti* as opposed to *syn* protonators, must necessarily come at a cost in terms of optimal interactions elsewhere.

Other well-characterized inhibitors of glycoside hydrolases, such as isofagomine (**3**) and 1-deoxynojirimycin (**4**), are not restrained to transition-state-mimicking ring conformations (in contrast to **1** and **2)** and most likely adopt the $^4C_1$ conformation in solution. In contrast, however, their conjugate acids are proposed to have positive charge at the site corresponding to that observed in the transition state (*13*). Their description as "transition-state analogues" remains a contentious issue and certainly requires quantification. **1** and **2** also contain a hydroxyl substituent at C2, which many glycosidase inhibitors do not. Given that the hydroxyl group at C2 is estimated to provide >40 kJ mol^{-1} to the stabilization of the transition state (*28*), this interaction is extremely important. Indeed, the nucleophile and the O2 substituent on the hydroximolactam inhibitors interact via a hydrogen bond between 2.5 and 2.8 Å. As mentioned previously, the carbonyl in the covalent intermediate complexes is rotated away from the saccharide to avoid steric clashes between F2 of the glycoside and Oϵ1, and thus no useful comparison can be made with the putative transition state, and alternative strategies for trapping need be considered (for example, see ref *46*).

The structure of Ssβ-Glc1 in complex with **1** and **2** contributes to the growing, but still limited, structural picture of glycosidase inhibition. The structure of the family GH1

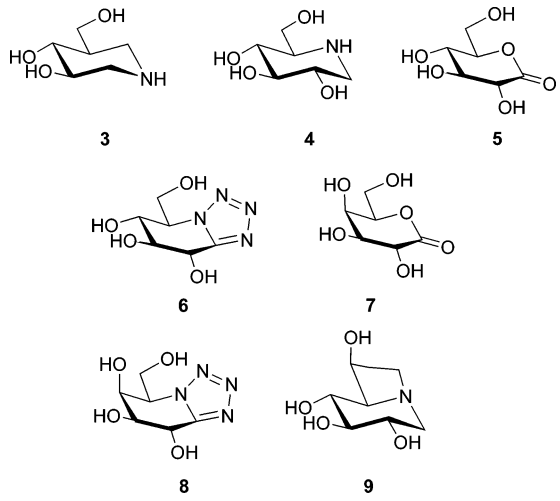

myrosinase has been deduced in complex with a number of proposed transition-state analogues. **1** was observed to bind in a "slightly distorted half-chair", with the nitrogen of the hydroximo group interacting with the oxygen of Gln187 (the residue equivalent to the acid/base glutamate in other family 1 hydrolases). D-Glucono-1,5-lactone (**5**) also binds as a distorted half-chair, with the O1 of the lactone in van der Waals' contact with the oxygen of Gln187, whereas gluco-

tetrazole (**6**) binds in a true half-chair conformation, with a nitrogen of the tetrazole hydrogen-bonding to the oxygen of the same glutamine residue (*47*). The *galacto* forms of these inhibitors, D-galactono-1,5-lactone (**7**) and galacto-tetrazole (**8**), were shown to bind to a family 2 β-galactosidase from *Escherichia coli*. The oxygen of the lactone group interacted with the acid/base residue in the enzyme. Both inhibitors were bound slightly rotated in comparison to intermediates in the process, to prevent steric clashes between C1 of the inhibitor and the nucleophile of the protein (*48*). The structure of a family 5 exo-β-(1,3)-glucanase from *Candida albicans* in complex with a putative transition-state mimic, castanospermine (**9**), showed that the inhibitor adopted a skewed-boat conformation, the presumed precursor to the transition state (*49*). The nitrogen atom (which is observed approximately halfway between the position expected for the endocyclic oxygen and anomeric carbon) interacts with the anionic oxygen atom of the nucleophile of the protein. A family 1 β-glucosidase from *T. maritima* bound to isofagomine (**3**) in a relaxed $^4C_1$ conformation, with an electrostatic interaction between the nitrogen and the carboxylate of the nucleophile and a Coulombic interaction with the acid/base glutamate. The structure with 1-deoxynojirimycin (**4**) was shown to bind in a near $^4C_1$ conformation, although C1 was upwardly displaced, meaning the nucleophile interacted with O2 and N5 (*13*).

Given the importance of glycosidase inhibition, both in the quest for therapeutic agents and in the need to understand transition-state recognition of these powerful catalysts, it is perhaps surprising just how few (*exo*)-glycosidase structures have been reported in complex with their respective (monosaccharide) inhibitors. It is only with an increase in structural information, coupled with thermodynamic and kinetic data, that a better profile of what makes a good transition state can be ascertained. Given the emerging picture of different enzymes harnessing conformationally different transition states (*50*), a more detailed analysis of what makes a good transition-state mimic should lead to a new generation of powerful and specific enzyme inhibitors.

REFERENCES

1. Wolfenden, R., Lu, X., and Young, G. (1998) Spontaneous Hydrolysis of Glycosides, *J. Am. Chem. Soc. 120*, 6814−6815.
2. Wolfenden, R., and Snider, M. J. (2001) The Depth of Chemical Time and the Power of Enzymes as Catalysts, *Acc. Chem. Rev. 34*, 938−945.
3. von Itzstein, M., Wu, W.-Y., Kok, G. B., Pegg, M. S., Dyason, J. C., Jin, B., Phan, T. V., Smythe, M. L., White, H. F., Oliver, S. W., Colman, P. M., Varghese, J. N., Ryan, D. M., Woods, J. M., Bethell, R. C., Hotham, V. J., Cameron, J. M., and Penn, C. R. (1993) Rational design of potent sialidase-based inhibitors of influenza virus replication, *Nature 363*, 418−423.
4. Henrissat, B., and Bairoch, A. (1996) Updating the sequence-based classification of glycosyl hydrolases, *Biochem. J. 316*, 695−696.
5. Aguilar, C. F., Sanderson, I., Moracci, M., Ciaramella, M., Nucci, R., Rossi, M., and Pearl, L. H. (1997) Crystal Structure of the β-Glycosidase from the Hyperthermophilic Archeon *Sulfolobus solfataricus*: Resilience as a Key Factor in Thermostability, *J. Mol. Biol. 271*, 789−802.
6. Hakulinen, N., Paavilainen, S., Korpela, T., and Rouvinen, J. (2000) The Crystal Structure of β-Glucosidase from *Bacillus circulans* sp. *alkalophilus*: Ability to Form Long Polymeric Assemblies, *J. Struct. Biol. 129*, 69−79.
7. Moracci, M., Ciaramella, M., and Rossi, M. (2001) β-Glycosidase from *Sulfolobus solfataricus*, *Methods Enzymol 330*, 201−215.
8. Sanz-Aparicio, J., Hermoso, J. A., Martínez-Ripoll, M., Lequerica, J. L., and Polaina, J. (1998) Crystal Structure of β-Glucosidase A from *Bacillus polymyxa*: Insights into the Catalytic Activity in Family 1 Glycosyl Hydrolases, *J. Mol. Biol. 275*, 491−502.
9. Wiesmann, C., Beste, G., Hengstenberg, W., and Schulz, G. E. (1995) The three-dimensional structure of 6-phospho-β-galactosidase from *Lactococcus lactis*, *Structure 3*, 961−968.
10. Barrett, T., Suresh, C. G., Tolley, S. P., Dodson, E. J., and Hughes, M. A. (1995) The crystal structure of a cyanogenic β-glucosidase from white clover, a family 1 glycosyl hydrolase, *Structure 3*, 951−960.
11. Czjzek, M., Cicek, M., Zamboni, V., Burmeister, W. P., Bevan, D. R., Henrissat, B., and Esen, A. (2001) Crystal structure of a monocotyledon (maize ZMGlu1) β-glucosidase and a model of its complex with *p*-nitrophenyl β-D-thioglucoside, *Biochem. J. 354*, 37−46.
12. Zouhar, J., Vévodová, J., Marek, J., Damborský, J., Su, X.-D., and Brzobohatý, B. (2001) Insights into the Functional Architecture of the Catalytic Center of a Maize β-Glucosidase Zm-p60.1, *Plant Physiol. 127*, 973−985.
13. Zechel, D. L., Boraston, A. B., Gloster, T., Boraston, C. M., Macdonald, J. M., Tilbrook, D. M. G., Stick, R. V., and Davies, G. J. (2003) Iminosugar Glycosidase Inhibitors: Structural and Thermodynamic Dissection of the Binding of Isofagomine and 1-Deoxynojirimycin to β-Glucosidases, *J. Am. Chem. Soc. 125*, 14313−14323.
14. Papandreou, G., Tong, M. K., and Ganem, B. (1993) Amidine, amidrazone and amidoxime derivatives of monosaccharide aldonolactams: synthesis and evaluation as glycosidase inhibitors, *J. Am. Chem. Soc. 115*, 11682−11690.
15. Vonhoff, S., Heightman, T. D., and Vasella, A. (1998) Inhibition of glycosidases by lactam oximes: Influence of the aglycon in disaccharide analogues, *Helv. Chim. Acta 81*, 1710−1725.
16. Ganem, B., and Papandreou, G. (1991) Mimicking the glucosidase transition state: shape/charge considerations, *J. Am. Chem. Soc. 113*, 8984−8985.
17. Hoos, R., Naughton, A. B., Thiel, W., Vasella, A., Weber, W., Rupitz, K., and Withers, S. G. (1993) D-Gluconhydroximo-1,5-lactam and related *N*-Arylcarbamates. Theoretical Calculations, Structure, Synthesis, and Inhibitory Effect on β-Glucosidases, *Helv. Chim. Acta 76*, 2666−2686.
18. Otwinowski, Z., and Minor, W. (1997) Macromolecular Crystallography, Part A, in *Methods in Enzymology* (Carter, C. W., Jr., Sweet, R. M., Eds.) Vol. 276, Academic Press, San Diego, CA.
19. Collaborative Computational Project Number 4. (1994) The *CCP*4 Suite: Programs for Protein Crystallography, *Acta Crystallogr. D 50*, 760−763.
20. Navaza, J. (1994) *AMoRe*: an Automated Package for Molecular Replacement, *Acta Crystallogr. A 50*, 157−163.
21. Brünger, A. T. (1992) Free *R* value: a novel statistical quantity for assessing the accuracy of crystal structures, *Nature 355*, 472−475.
22. Murshudov, G. N., Vagin, A. A., and Dodson, E. J. (1997) Refinement of Macromolecular Structures by the Maximum-Likelihood Method, *Acta Crystallogr. D 53*, 240−255.
23. Lamzin, V. S., and Wilson, K. S. (1993) Automated refinement of protein models, *Acta Crystallogr. D 49*, 129−147.
24. Laskowski, R. A., MacArthur, M. W., Moss, D. S., and Thornton, J. M. (1993) PROCHECK: a program to check the stereochemical quality of protein structures, *J. Appl. Crystallogr. 26*, 283−291.
25. Moracci, M., Trincone, A., Perugino, G., Ciaramella, M., and Rossi, M. (1998) Restoration of the Activity of Active-Site Mutants of the Hyperthermophilic β-Glycosidase from *Sulfolobus solfataricus*: Dependence of the Mechanism on the Action of External Nucleophiles, *Biochemistry 37*, 17262−17270.
26. Leatherbarrow, R. J. (2001) *GraFit Version 5*, Erithacus Software Ltd., Horley, UK.
27. Moracci, M., Capalbo, L., Ciaramella, M., and Rossi, M. (1996) Identification of two glutamic acid residues essential for catalysis in the β-glycosidase from the thermoacidphilic archaeon *Sulfolobus solfataricus*, *Protein Eng. 9*, 1191−1195.
28. Namchuk, M. N., and Withers, S. G. (1995) Mechanism of *Agrobacterium* β-Glucosidase: Kinetic Analysis of the Role of Noncovalent Enzyme/Substrate Interactions, *Biochemistry 34*, 16194−16202.
29. Legler, G. (1990) Glycoside hydrolases: Mechanistic information from studies with reversible and irreversible inhibitors, *Adv. Carbohydr. Chem. Biochem. 48*, 319−384.
30. Kempton, J. B., and Withers, S. G. (1992) Mechanism of *Agrobacterium* β-Glucosidase: Kinetic Studies, *Biochemistry 31*, 9961−9969.

31. Heightman, T. D., and Vasella, A. (1999) Recent insights into inhibition, structure, and mechanism of configuration-retaining glycosidases, *Angew. Chem., Int. Ed. 38*, 750−770.
32. Vasella, A., Davies, G., and Böhm, M. (2002) Glycosidase Mechanisms, *Curr. Opin. Chem. Biol. 6*, 619−629.
33. Vocadlo, D. J., Davies, G. J., Laine, R., and Withers, S. G. (2001) Catalysis by hen egg-white lysozyme proceeds via a covalent intermediate, *Nature 412*, 835−838.
34. Ducros, V. M.-A., Zechel, D. L., Murshudov, G. N., Gilbert, H. J., Szabó, L., Stoll, D., Withers, S. G., and Davies, G. J. (2002) Substrate Distortion by a β-Mannanase: Snapshots of the Michaelis and Covalent-Intermediate Complexes Suggest a $B_{2,5}$ Conformation for the Transition State, *Angew. Chem., Int. Ed. 41*, 2824−2827.
35. Sidhu, G., Withers, S. G., Nguyen, N. T., McIntosh, L. P., Ziser, L., and Brayer, G. D. (1999) Sugar ring distortion in the glycosyl-enzyme intermediate of a family G/11 xylanase, *Biochemistry 38*, 5346−54.
36. Sabini, E., Sulzenbacher, G., Dauter, M., Dauter, Z., Jorgensen, P. L., Schülein, M., Dupont, C., Davies, G. J., and Wilson, K. S. (1999) Catalysis and specificity in enzymatic glycoside hydrolysis: a ^{2,5}B conformation for the glycosyl−enzyme intermediate revealed by the structure of the *Bacillus agaradhaerens* family 11 xylanase, *Chem. Biol. 6*, 483−492.
37. Uitdehaag, J. C. M., Mosi, R., Kalk, K. H., van der Veen, B. A., Dijkhuizen, L., Withers, S. G., and Dijkstra, B. W. (1999) Catalysis in the α-amylase family−X-ray structures along the reaction pathway of cyclodextrin glycosyltransferase, *Nat. Struct. Biol. 6*, 432−436.
38. Perugino, G., Trincone, A., Giordano, A., van der Oost, J., Kaper, T., Rossi, M., and Moracci, M. (2003) Activity of Hyperthermophilic Glycosynthase Is Significantly Enhanced at Acidic pH, *Biochemistry 42*, 8484−8493.
39. Trincone, A., Perugino, G., Rossi, M., and Moracci, M. (2000) A Novel Thermophilic Glycosynthase That Effects Branching Glycosylation, *Bioorg. Med. Chem. Lett. 10*, 365−368.
40. Mayer, C., Zechel, D. L., Reid, S. P., Warren, R. A. J., and Withers, S. G. (2000) The E358S mutant of Agrobacterium sp. β-glucosidase is a greatly improved glycosynthase, *FEBS Lett. 466*, 40−44.
41. Mackenzie, L. F., Wang, Q., Warren, R. A. J., and Withers, S. G. (1998) Glycosynthases: mutant glycosidases for oligosaccharide synthesis, *J. Am. Chem. Soc. 120*, 5583−5584.
42. Mark, B. L., Vocadlo, D. J., Zhao, D., Knapp, S., Withers, S. G., and James, M. N. G. (2001) Biochemical and Structural Assessment of the 1-*N*-Azasugar GalNAc-isofagomine as a Potent Family 20 β-*N*-Acetylhexosaminidase Inhibitor, *J. Biol. Chem. 276*, 42131−42137.
43. Mark, B. L., Mahuran, D. J., Cherney, M. M., Zhao, D. L., Knapp, S., and James, M. N. G. (2003) Crystal structure of human beta-hexosaminidase B: Understanding the molecular basis of Sandhoff and Tay-Sachs disease, *J. Mol. Biol. 327*, 1093−1109.
44. Corbett, K., Fordham-Skelton, A. P., Gatehouse, J. A., and Davis, B. G. (2001) Tailoring the substrate specificity of the β-glycosidase from the thermophilic archaeon *Sulfolobus solfataricus*, *FEBS Lett. 509*, 355−360.
45. Hoos, R., Vasella, A., Rupitz, K., and Withers, S. G. (1997) D-Glyconhydroxyimolactams strongly inhibit α-glycosidases, *Carbohydr. Res. 298*, 291−298.
46. Notenboom, V., Birsan, C., Nitz, M., Rose, D. R., Warren, R. A. J., and Withers, S. G. (1998) Insights into transition state stabilisation of the β-1,4 glycosidase Cex by covalent intermediate accumulation in active site mutants, *Nat. Struct. Biol. 5*, 812−818.
47. Burmeister, W. P., Cottaz, S., Rollin, P., Vasella, A., and Henrissat, B. (2000) High-Resolution X-ray Crystallography Shows That Ascorbate Is a Cofactor for Myrosinase and Substitutes for the Function of the Catalytic Base, *J. Biol. Chem. 275*, 39385−39393.
48. Juers, D. H., Heightman, T. D., Vasella, A., McCarter, J. D., Mackenzie, L., Withers, S. G., and Matthews, B. W. (2001) A Structural View of the Action of *Escherichia coli* (*lac*Z) β-Galactosidase, *Biochemistry 40*, 14781−14794.
49. Cutfield, S. M., Davies, G. J., Murshudov, G., Anderson, B. F., Moody, P. C. E., Sullivan, P. A., and Cutfield, J. F. (1999) The Structure of the Exo-β-(1,3)-Glucanase from *Candida albicans* in Native and Bound Forms: Relationship between a Pocket and Groove in Family 5 Glycosyl Hydrolases, *J. Mol. Biol. 294*, 771−783.
50. Davies, G. J., Ducros, V. M.-A., Varrot, A., and Zechel., D. L. (2003) Mapping the conformational itinerary of β-glycosidases by X-ray crystallography, *Biochem. Soc. Trans. 31*, 523−527.
51. Kraulis, P. J. (1991) MOLSCRIPT: a program to produce both detailed and schematic plots of protein structures, *J. Appl. Crystallogr. 24*, 946−950.
52. Esnouf, R. M. (1997) An extensively modified version of MolScript that includes greatly enhanced coloring capabilities, *J. Mol. Graphics Modell. 15*, 132−134.

BI049666M